Near-infrared resonance-mediated chirp control of a coherently generated broadband deep-ultraviolet spectrum

Leonid Rybak, Lev Chuntonov,[*] Andrey Gandman,[†] Naser Shakour, and Zohar Amitay[‡]

The Shirlee Jacobs Femtosecond Laser Research Laboratory, Schulich Faculty of Chemistry, Technion - Israel Institute of Technology, Haifa 32000, Israel

(Received 15 June 2011; published 12 September 2011)

We investigate the use of shaped near-infrared (NIR) femtosecond pulses to control the generation of coherent broadband deep-ultraviolet (DUV) radiation in an atomic resonance-mediated (2+1) three-photon excitation to a broad far-from-resonance continuum. Previously, we have shown control over the total emitted DUV yield. Here, we experimentally demonstrate phase control over the spectral characteristics (central frequency and bandwidth) of the emitted broadband DUV radiation. It is achieved by tuning the linear chirp applied to the exciting NIR femtosecond pulse. The study is conducted with Na vapor.

DOI: 10.1103/PhysRevA.84.035401 PACS number(s): 32.80.Qk, 32.80.Wr, 42.65.Re

Optical femtosecond coherent control of multiphoton processes [1–25] exploits the broad coherent spectrum of femtosecond pulses to control state-to-state transition probabilities by manipulating the interferences among multiple photoinduced state-to-state pathways. The control handle is the shape of the exciting pulse that is optically manipulated by pulse shaping techniques [26,27]. In femtosecond coherent phase control the pulse shape is tailored by altering the phases of the different spectral components of the broadband pulse. The initial identification of the interfering pathways and their interference mechanism allows us to employ a rational control approach that has been shown to be very successful in a variety of nonresonant and resonance-mediated multiphoton processes in atoms and molecules [1–25]. For completeness, it worth mentioning that coherent phase control of multiphoton excitation and ionization processes has also been demonstrated by other means, including narrow-band optical light [2,3] and microwave radiation [28,29].

Recently, we have used shaped near-infrared (NIR) femtosecond pulses to phase control the total yield of coherent deep-ultraviolet (DUV) radiation generated in an atomic resonance-mediated (2+1) three-photon excitation [23]. The resonance-mediated nature of the excitation provides a much higher degree of control over the emitted DUV radiation as compared to a completely nonresonant excitation. The first case that we have investigated is the resonance-mediated (2+1) three-photon generation of a narrow-band coherent DUV radiation due to a single excited real bound state that is resonantly accessed at the three-photon excitation level. Then, we have extended the control to the case of generating broadband DUV radiation via a resonance-mediated excitation to a broad far-from-resonance continuum with no resonant access to any real state at the three-photon excitation level. As mentioned, this previous experimental control has been over the total emitted DUV yield. Here, we experimentally demonstrate phase control over the spectral characteristics (central frequency and bandwidth) of the emitted broadband DUV radiation. It is achieved by tuning the linear chirp applied to the exciting NIR femtosecond pulse.

Conceptually, from a fundamental coherent-control point of view, controlling the total yield of the narrow-band coherent DUV radiation [23] is equivalent to controlling the total population excited to the single (real) target state at the three-photon excitation level [15]. The extension of the DUV-yield control to the case of broadband DUV radiation [23] corresponds then to extending the population control to controlling the total population simultaneously excited to a continuous manifold of multiple (virtual) target states. Along the same conceptual line, the present control over the generated broadband DUV spectrum corresponds then to controlling the population branching ratio among these multiple target states, i.e., controlling their relative final populations.

Figure 1(a) shows the atomic broadband excitation scheme considered here, involving an initial ground state $|g\rangle$ and an excited state $|r\rangle$ that are of one symmetry and a manifold of excited states $|v\rangle$ that are of another symmetry. Irradiation with a shaped NIR femtosecond pulse induces a resonance-mediated (2+1) three-photon excitation from $|g\rangle$ via $|r\rangle$ to a broad far-from-resonance continuum, resulting in a time-dependent atomic polarization that drives the generation of a corresponding shaped coherent broadband DUV radiation. The last coherent emission step is associated with a corresponding de-excitation to $|g\rangle$. Along this whole photoinduced process the $|v\rangle$ states are accessed nonresonantly and provide the $|g\rangle$-$|r\rangle$ nonresonant two-photon couplings at the one- and three-photon excitation energies.

The generated DUV spectral field $E_{\mathrm{out}}(\Omega_{\mathrm{DUV}})$ at frequency Ω_{DUV} is given by [23]

$$E_{\mathrm{out}}(\Omega_{\mathrm{DUV}}) \propto A^{(2+1)\text{on-res}}(\Omega_{\mathrm{DUV}}) + A^{(2+1)\text{near-res}}(\Omega_{\mathrm{DUV}}) , \quad (1)$$

$$A^{(2+1)\text{on-res}}(\Omega_{\mathrm{DUV}}) = i\pi A^{(2)}(\omega_{r,g}) E(\Omega_{\mathrm{DUV}} - \omega_{r,g}) , \quad (2)$$

$$A^{(2+1)\text{near-res}}(\Omega_{\mathrm{DUV}}) = -\mathrm{P}\int_{-\infty}^{\infty} \frac{1}{\delta} A^{(2)}(\omega_{r,g} - \delta) \times E(\Omega_{\mathrm{DUV}} - \omega_{r,g} + \delta) d\delta , \quad (3)$$

$$A^{(2)}(\xi) = \int_{-\infty}^{\infty} E(\omega_{\mathrm{NIR}}) E(\xi - \omega_{\mathrm{NIR}}) d\omega_{\mathrm{NIR}} , \quad (4)$$

[*]Present address: Department of Chemical Physics, Weizmann Institute of Science, Rehovot 76100, Israel.

[†]Present address: Department of Chemistry, University of California, Berkeley, CA 94720, USA.

[‡]amitayz@technion.ac.il

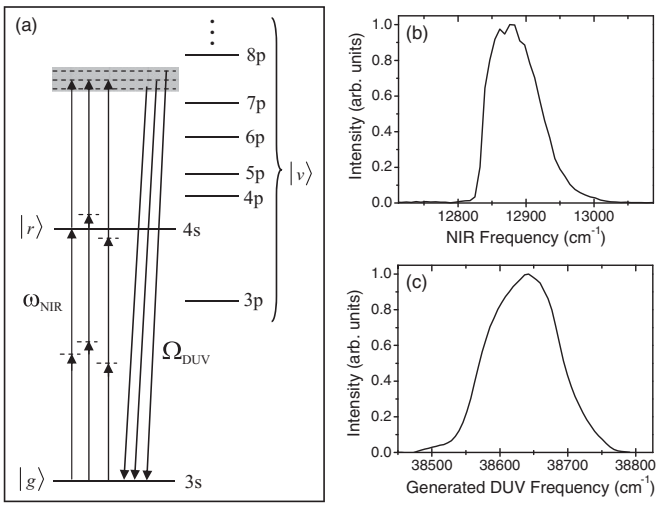

FIG. 1. (a) Na excitation scheme for the generation of coherent broadband DUV radiation by shaped NIR femtosecond pulses via resonance-mediated (2+1) three-photon excitation to a broad far-from-resonance continuum. (b) The Spectrum of the driving NIR femtosecond pulses. (c) The Spectrum of the coherent broadband DUV radiation generated by the NIR transform-limited pulse.

with $\omega_{r,g}$ being the $|g\}$-$|r\rangle$ transition frequency and P being the Cauchy principal value. The $E(\omega_{\rm NIR}) \equiv |E(\omega_{\rm NIR})| \exp[-i\,\Phi(\omega_{\rm NIR})]$ is the NIR spectral field of the excitation pulse, with $|E(\omega_{\rm NIR})|$ and $\Phi(\omega_{\rm NIR})$ being, respectively, the spectral amplitude and phase of frequency $\omega_{\rm NIR}$. The transform-limited (TL) pulse corresponds to $\Phi(\omega_{\rm NIR}) = 0$. The spectral intensity generated at $\Omega_{\rm DUV}$ is $I_{\rm out}(\Omega_{\rm DUV}) \propto |E_{\rm out}(\Omega_{\rm DUV})|^2$.

As can be concluded from the above frequency-domain formulation and is illustrated in Fig. 1(a), the DUV field $E_{\rm out}(\Omega_{\rm DUV})$ generated at frequency $\Omega_{\rm DUV}$ results from the interferences among all the possible resonance-mediated three-photon excitation pathways from $|g\rangle$ to the excitation energy corresponding to $\Omega_{\rm DUV}$ [23]. A pathway of detuning δ from $|r\rangle$ involves a nonresonant absorption of two photons with a frequency sum of $\omega_{r,g} - \delta$ and the absorption of a third complementary photon of frequency $\Omega_{\rm DUV} - (\omega_{r,g} - \delta)$. The on-resonant ($\delta = 0$) and near-resonant ($\delta \neq 0$) pathways reaching the energy of $\Omega_{\rm DUV}$ are interfered separately in $A^{(2+1)\text{on-res}}(\Omega_{\rm DUV})$ and $A^{(2+1)\text{near-res}}(\Omega_{\rm DUV})$, respectively. They are expressed using the parameterized amplitude $A^{(2)}(\xi)$ interfering all the nonresonant two-photon pathways of frequency sum ξ, each composed of photon pair $\omega_{\rm NIR}$ and $\xi - \omega_{\rm NIR}$. As the exciting NIR field $E(\omega_{\rm NIR})$ controls the amplitudes and phases of the different interfering three-photon pathways, it also controls the emitted DUV field $E_{\rm out}(\Omega_{\rm DUV})$ at each $\Omega_{\rm DUV}$ and the corresponding intensity $I_{\rm out}(\Omega_{\rm DUV})$. The relative intensity among the different DUV frequencies determines the shape of the emitted DUV spectrum, which is the control objective of the present study.

The model system is the Na atom [Fig. 1(a)], with the $3s$ ground state as $|g\rangle$, the $4s$ state as $|r\rangle$, and the manifold of p states as $|v\rangle$. The $3s$-$4s$ transition frequency is $\omega_{r,g} \equiv \omega_{4s,3s} = 25\,740$ cm^{-1} (two 777-nm photons). The sodium is irradiated with phase-shaped linearly polarized NIR femtosecond pulses having a spectrum peaked at $\omega_{\rm NIR,0} = 12\,876$ cm^{-1} (776.6 nm) with 88 cm^{-1} bandwidth, as shown in Fig. 1(b). The TL peak intensity is $I_{\rm TL} \sim 3 \times 10^{10}$ W/cm^2. The NIR spectrum results from blocking an original spectrum at its lower-frequency edge to prevent three-photon resonant access to the $7p$ state [$\omega_{7p,4s} = 12\,801$ cm^{-1} (781.2 nm)], which is undesired for generating DUV radiation of a broadband nature. The interaction with the NIR excitation pulse leads to the generation of a coherent broadband DUV radiation. Experimentally, a sodium vapor in a heated cell at 900 K with Ar buffer gas is irradiated with the NIR laser pulses after they undergo shaping in a setup incorporating a pixelated liquid-crystal spatial light phase modulator. The shaping resolution is 2.05 cm^{-1}. The coherent DUV radiation emitted in the propagation direction of the NIR beam is measured using a DUV spectrometer coupled to a time-gated camera system. The corresponding overall DUV spectral resolution is 35 cm^{-1} (0.23 nm), with 5.8-cm^{-1} spectral width of each camera pixel. Up to the NIR TL peak intensity $I_{\rm TL}$ of our experiment, the DUV generation efficiency exhibits a cubic dependence on $I_{\rm TL}$, indicating the third-order perturbative regime associated with Eqs. (1) to (4).

Figure 1(c) shows the measured coherent DUV spectrum generated by the NIR TL pulse. As seen, it is of a broadband nature with a bandwidth of 125 cm^{-1} around its maximum at $\Omega_{\rm DUV} = 38\,642$ cm^{-1} (258.78 nm). After deconvoluting the measurement resolution, the DUV spectral bandwidth amounts to 120 cm^{-1}. The peak DUV frequency of 38 642 cm^{-1} corresponds to $\omega_{4s,3s}$ plus a frequency of 12 902 cm^{-1} that is around the peak NIR frequency $\omega_{\rm NIR,0}$. As seen from Eqs. (2) to (4), the on-resonant amplitude $A^{(2+1)\text{on-res}}(\Omega_{\rm DUV})$ is, by definition, maximal at $\Omega_{\rm DUV} = \omega_{4s,3s} + \omega_{\rm NIR,0}$, while the peak location of the near-resonant amplitude $A^{(2+1)\text{near-res}}(\Omega_{\rm DUV})$ can deviate from it according to the specific NIR excitation spectrum.

As a first work on controlling the spectral characteristics of broadband DUV radiation generated via resonance-mediated shaped NIR femtosecond excitation, we have chosen to use here linearly chirped NIR pulses having quadratic spectral phase patterns $\Phi(\omega_{\rm NIR}) = \frac{1}{2}k_{\rm chirp}(\omega_{\rm NIR} - \omega_{\rm NIR,0})^2$ of variable chirp parameter $k_{\rm chirp}$. The value of $k_{\rm chirp}$ is tuned from negative to positive values, with the zero value $k_{\rm chirp} = 0$ corresponding to the NIR TL pulse.

Figure 2(a) presents the complete set of the experimentally generated chirp-controlled DUV spectra. The results are presented as a color-coded map of the spectral intensity $I_{\rm out}(\Omega_{\rm DUV}, k_{\rm chirp})$ measured at each DUV frequency $\Omega_{\rm DUV}$ as a function of the $k_{\rm chirp}$ value applied to the generating linearly chirped NIR pulse. Each DUV spectrum at a particular value of $k_{\rm chirp}$ is normalized (independently) by its maximal intensity. The experimental chirp dependence of the peak frequency (i.e., the frequency of maximal intensity) and bandwidth [full width at half maximum (FWHM)] of the generated DUV spectrum, as obtained from the map data, are shown (as circles) in Figs. 2(b) and 2(c). The corresponding theoretical results, which are the outcome of numerical calculations based on Eqs. (1) to (4) that have been followed by a convolution with the DUV spectral measurement resolution, are also shown (as lines). As seen, the calculated results are in reasonable agreement with the experimental results. A possible source

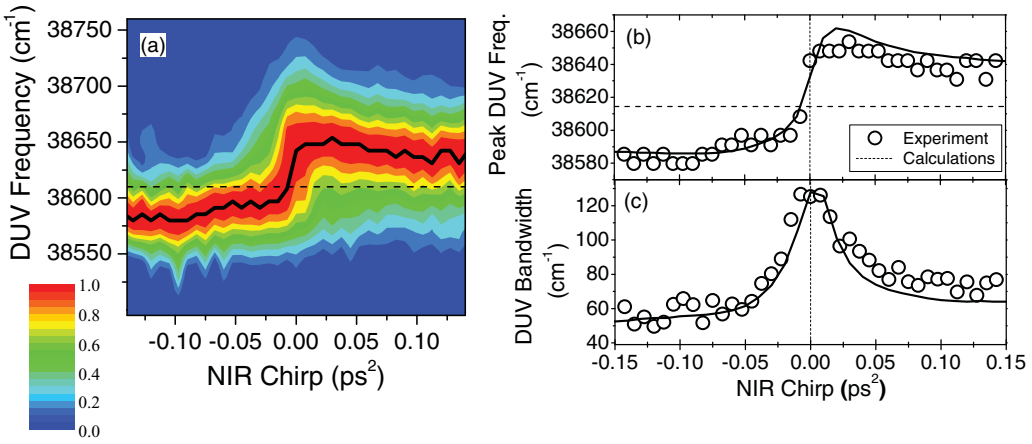

FIG. 2. (Color online) Results for the NIR resonance-mediated chirp control of the broadband DUV radiation coherently generated in Na by linearly chirped NIR femtosecond pulses. (a) Experimental results for the spectral intensity (color coded) measured at each DUV frequency as a function of the applied NIR chirp. Each DUV spectrum at a given chirp value is normalized (independently) by its maximal intensity. (b), (c) Experimental results (circles) for the NIR-chirp dependence of the measured peak DUV frequency and DUV bandwidth (FWHM), respectively, as obtained from the data of (a). Corresponding calculated results (lines) are also shown. The dashed lines in (a) and (b) indicate the DUV frequency of $3\omega_{4s,3s}/2$ (see text).

for the corresponding existing difference might be the fact that complicated effects of shaped-pulse propagation and phase matching are not included in the calculations.

As the value of k_{chirp} is experimentally tuned from negative to positive values, the peak DUV frequency $\Omega_{\text{DUV},0}$ changes from around 38 580 cm^{-1} when $k_{\text{chirp}} \leqslant -0.1$ ps^2 to around 38 635 cm^{-1} when $k_{\text{chirp}} \geqslant +0.1$ ps^2, with a value of 38 642 cm^{-1} when $k_{\text{chirp}} = 0$. The change of $\Omega_{\text{DUV},0}$ takes place mostly at the region of small chirp values around zero chirp. Dashed lines of reference, which we refer to further below, are indicated in Figs. 2(a) and 2(b) at the DUV frequency of $3\omega_{4s,3s}/2$ (38 610 cm^{-1}). The measured DUV bandwidth $\Delta\Omega_{\text{DUV}}$ amounts to about 125 cm^{-1} around zero chirp and decreases continuously down to 55–75 cm^{-1} at the larger negative and positive chirps of $|k_{\text{chirp}}| \geqslant 0.1$ ps^2. After deconvoluting the experimental resolution, the corresponding values are about 120 cm^{-1} and 40–65 cm^{-1}, respectively. The chirp dependence of $\Delta\Omega_{\text{DUV}}$ is nearly symmetrical around $k_{\text{chirp}} = 0$. As described above, all these specific chirp-dependent values of $\Omega_{\text{DUV},0}$ and $\Delta\omega_{\text{DUV}}$, as well as their tunability range, result from the specific NIR excitation spectrum used here.

A highly intuitive qualitative understanding of these chirp dependencies is actually obtained by combining the frequency-domain picture of Eqs. (1) to (4) with the picture of the so-called joint time-frequency domain. Under this framework, zero chirp (a TL pulse) corresponds to the simultaneous arrival of all the spectral pulse frequencies, while positive and negative chirps correspond to the cases where lower frequencies arrive, respectively, before or after higher frequencies. The temporal separation between two different frequencies increases as the chirp magnitude increases. With regard to the Na excitation, the resonance-mediated (2+1) three-photon excitation to a given total energy of Ω_{DUV} is expected to be of large amplitude, leading to high DUV intensity at Ω_{DUV}, once the third-photon absorption occurs shortly after the excitation of the intermediate $4s$ state. Based on Eq. (4) of $A^{(2)}(\xi \approx \omega_{4s,3s})$, such $4s$ excitation occurs by absorbing all the NIR photon pairs having their frequency sum close to $\omega_{4s,3s}$, i.e., their frequencies are symmetric around $\sim\omega_{4s,3s}/2$. Thus, the efficient transient $4s$ excitation can be associated with a narrow time window around the arrival time of the pulse frequency $\omega_{4s,3s}/2$. Hence, overall, efficient resonance-mediated excitation is expected for the energies of $\Omega_{\text{DUV}} \approx \omega_{4s,3s} + \omega_{\text{NIR},3}$ with $\omega_{\text{NIR},3}$ being either larger or smaller than $\omega_{4s,3s}/2$ according to whether the NIR chirp is positive or negative, respectively. Consequently, the positive and negative NIR chirps are expected to lead to efficient DUV generation mostly at DUV frequencies that are either larger or smaller than $3\omega_{4s,3s}/2$, respectively. Also, since larger chirp magnitude leads to larger temporal spread of the pulse frequencies such that fewer frequencies arrive within the time window of efficient excitation, the generated DUV bandwidth is expected to be the largest for NIR chirps around zero and to decrease toward a constant level as the chirp magnitude increases. Indeed, as seen in Figs. 2(a) to 2(c), the observed chirp-dependent results follow this qualitatively-predicated behavior.

In conclusion, we have experimentally demonstrated NIR-chirp control over the broadband spectrum (central frequency and bandwidth) of the DUV radiation that is coherently generated by shaped femtosecond NIR pulses in a resonance-mediated (2+1) three-photon excitation of atomic sodium to a broad far-from-resonance continuum. This is complementary to the previously demonstrated control over the generated DUV yield.

This research was supported by The Israel Science Foundation (Grant No. 1450/10), by The James Franck Program in Laser Matter Interaction, by The P. and E. Nathan Research Fund, and by The Technion V.P.R. Fund.

[1] D. J. Tannor, R. Kosloff, and S. A. Rice, J. Chem. Phys. **85**, 5805 (1986).
[2] M. Shapiro and P. Brumer, *Principles of the Quantum Control of Molecular Processes* (Wiley, Hoboken, NJ, 2003).
[3] R. J. Gordon and S. A. Rice, Annu. Rev. Phys. Chem. **48**, 601 (1997).
[4] H. Rabitz, R. de Vivie-Riedle, M. Motzkus, and K. Kompa, Science **288**, 824 (2000).
[5] P. Nuernberger, G. Vogt, T. Brixner, and G. Gerber, Phys. Chem. Chem. Phys. **9**, 2470 (2007).
[6] M. Dantus and V. V. Lozovoy, Chem. Rev. **104**, 1813 (2004).
[7] Y. Silberberg, Annu. Rev. Phys. Chem. **60**, 277 (2009).
[8] D. Meshulach and Y. Silberberg, Nature (London) **396**, 239 (1998).
[9] A. Präkelt, M. Wollenhaupt, C. Sarpe-Tudoran, and T. Baumert, Phys. Rev. A **70**, 063407 (2004).
[10] D. J. Maas, C. W. Rella, P. Antoine, E. S. Toma, and L. D. Noordam, Phys. Rev. A **59**, 1374 (1999).
[11] N. Dudovich, B. Dayan, S. M. Gallagher Faeder, and Y. Silberberg, Phys. Rev. Lett. **86**, 47 (2001).
[12] B. Chatel, J. Degert, S. Stock, and B. Girard, Phys. Rev. A **68**, 041402 (2003).
[13] B. Chatel, J. Degert, and B. Girard, Phys. Rev. A **70**, 053414 (2004).
[14] L. Chuntonov, L. Rybak, A. Gandman, and Z. Amitay, Phys. Rev. A **77**, 021403 (2008).
[15] A. Gandman, L. Chuntonov, L. Rybak, and Z. Amitay, Phys. Rev. A **75**, 031401 (2007).
[16] Z. Amitay, A. Gandman, L. Chuntonov, and L. Rybak, Phys. Rev. Lett. **100**, 193002 (2008).
[17] N. T. Form, B. J. Whitaker, and C. Meier, J. Phys. B **41**, 074011 (2008).
[18] H. U. Stauffer, J. B. Ballard, Z. Amitay, and S. R. Leone, J. Chem. Phys. **116**, 946 (2002).
[19] X. Dai, Eliza-Beth W. Lerch, and S. R. Leone, Phys. Rev. A **73**, 023404 (2006).
[20] N. Dudovich, D. Oron, and Y. Silberberg, Nature (London) **418**, 512 (2002).
[21] S. H. Lim, A. G. Caster, and S. R. Leone, Phys. Rev. A **72**, 041803 (2005).
[22] B. von Vacano and M. Motzkus, Phys. Chem. Chem. Phys. **10**, 681 (2008).
[23] L. Rybak, L. Chuntonov, A. Gandman, N. Shakour, and Z. Amitay, Opt. Express **16**, 21738 (2008).
[24] C. Trallero-Herrero, J. L. Cohen, and T. Weinacht, Phys. Rev. Lett. **96**, 063603 (2006).
[25] A. Lindinger, C. Lupulescu, M. Plewicki, F. Vetter, A. Merli, S. M. Weber, and L. Wöste, Phys. Rev. Lett. **93**, 033001 (2004).
[26] A. M. Weiner, Rev. Sci. Instrum. **71**, 1929 (2000).
[27] T. Brixner and G. Gerber, Opt. Lett. **26**, 557 (2001).
[28] L. Sirko and P. M. Koch, Phys. Rev. Lett. **89**, 274101 (2002).
[29] P. M. Koch, S. A. Zelazny, and L. Sirko, J. Phys. B **36**, 4755 (2003).